2018 15th International Conference on
Control, Automation, Robotics and Vision (ICARCV)
Singapore, November 18-21, 2018

Parameter Identification of Blimp Dynamics through Swinging Motion

Qiuyang Tao, Jaeseok Cha, Mengxue Hou, and Fumin Zhang

Abstract— **Indoor miniature autonomous blimp (MAB) is a small-sized aerial platform with outstanding safety and flight endurance. A detailed six-degree-of-freedom (6DOF) dynamics model is critical for controller design and motion simulation. This paper presents the identification of the rotation-related parameters of the blimp dynamics model through swing motion of the robot. A pendulum-like grey box model is constructed to identify the parameters from physical measurements and system identification experiments. The pendulum-like dynamics model with identified parameters is then linearized for future controller design and validated with experimental data.**

I. INTRODUCTION

Indoor aerial robots are gaining increasing attention owing to their promising potential for applications including infrastructure inspection, warehouse management, and agriculture automation. Human-robot interaction with indoor airborne robots is a growing research trend in recent years [1]. However, most existing platforms such as quadcopters, have fast-spinning propellers which may cause safety concerns in human-occupied indoor environments. Besides, these platforms usually have short flight endurance, which poses limitations to their applications. Therefore, a safer robot that can fly for a longer time is increasingly needed.

Lighter than air robots (LTARs) keep themselves aloft without the need for motor action. Hence, LTARs have significantly extended endurance, and are well-suited to many applications that require sustained airborne presence [2]. However, size of LTARs is usually large to obtain sufficient amount of buoyancy [3]. As a consequence, most LTARs are designed for outdoor applications instead of indoor purposes.

We develop Georgia Tech Miniature Autonomous Blimp (GT-MAB), a cost-effective LTAR specifically designed for indoor environments. As shown in Fig. 1, GT-MAB is cushioned with a helium-filled envelop, making the robot safe to fly indoors, causing no threat to human and the surroundings even with collisions. With the lifting force provided by air buoyancy, GT-MAB has flight endurance for more than 2 hours [4], [5], [6]. Moreover, the modular design of GT-MAB makes the system expandable for a variety of tasks including environmental mapping and human-robot interaction [6], [7].

The research work is supported by ONR grants N00014-09-1-1074 and N00014-10-10712 (YIP), and NSF grants ECCS-0841195 (CAREER), CNS-0931576, and OCE-1032285.

Q. Tao and M. Hou are with School of Electrical and Computer Engineering, Georgia Institute of Technology, Atlanta, GA 30332, USA qiuyang, mengxue@gatech.edu

J. Cha is with School of Mechanical Engineering, Georgia Institute of Technology, Atlanta, GA 30313, USA jscha28@gatech.edu

F. Zhang is with Faculty of Electrical and Computer Engineering, Georgia Institute of Technology, Atlanta, GA 30332, USA fumin@gatech.edu

Fig. 1. GT-MAB assembly (left) and gondola with all electronics (right).

A detailed six-degree-of-freedom dynamics model is critical for the stable flight of GT-MAB. Our previous work identified the dynamics of the translational and steering motion of GT-MAB, and designed an autopilot based on the identified model [6]. However, this work did not investigate all of the rotational dynamics, namely pitch and roll movement of GT-MAB. As a consequence, lateral and longitudinal oscillation is often observed while GT-MAB is in flight. This undesirable oscillation has impacts on most applications of GT-MAB. The onboard sensors usually have directionality, and oscillation could cause inaccurate readings. Moreover, the video stream from the onboard camera also suffers from the unstable movement. Mechanical gimbals can be installed on aerial robots to stabilize the sensors [8], but such a device may exceed the payload of indoor miniature blimps. Besides the interference to the sensors, the oscillation consumes more energy and might cause people to feel less comfortable interacting with the robot. Therefore, identifying the rotation-related dynamics of GT-MAB is crucial for getting the 6DOF model of the robot, and to eventually eliminate the undesirable oscillation.

The oscillation has long been noticed by balloonists for outdoor airships, and the 6DOF modeling for these large-sized vehicles is widely available [9], [10]. Unfortunately, due to the unique mechatronic design and slow-speed operation of GT-MAB, existing model identification methods for outdoor airships, such as CFD simulation and wind tunnel testing [11], [12], [13], are hard to directly apply. Outdoor airships usually have cigar-shaped body and tail fins to control their attitude and reduce the oscillation during flight. In contrast, the envelop of GT-MAB is chosen to be highly optimized for indoor applications, and does not have cigar-shaped envelop or tail fins. Besides, hovering and low-speed flying is the most common operating scenario for GT-MAB, while the outdoor airships are mainly designed for cruising. Therefore, the dynamics model of GT-MAB needs to be identified with different approaches.

Due to the limitations including light-weight mechatronics, miniature indoor blimps are not widely available until recently. Only a few projects address the modeling and control of the indoor blimps with sizes slightly larger than GT-MAB. The work [14] compared PID and fuzzy logic algorithms for altitude control, and presented a fuzzy logic controller for collision avoidance. Authors of the work [15] presented a biologically based flight controller with visual information from two camera inputs. PID controllers are designed in the work [16], [3], and [17] for motion control and landing. Cooperative control of multiple neural networks are reported in the work [18] for the robustness with mechanical failures. The work [19] presented a behavior-based navigation system. However, dynamics model of the blimp is not discussed in these works. The work [20] presented the dynamics model of a miniature blimp, and studied the control strategy under wind disturbance. Similarly, both dynamics model and controller design are discussed in the work [21]. However, parameter identification of the dynamics model is not presented in these two literatures. The work [22] identified the parameters of the dynamics model, and designed controllers for indoor blimps. However, only the altitude-related modeling and control is presented. The work [23] presented the modeling and identification of an indoor blimp with hull-shaped envelop. However, some parameters are theoretically determined with the specific geometry of the envelop. Authors of the work [24] observed that the swinging motion of an indoor blimp is acting as a pendulum. However, modeling of the pendulum-like oscillation is not discussed.

In this work, we extend the existing efforts by identifying the rotation-related dynamics of GT-MAB through swing motion. A nonlinear pendulum-like grey box model is constructed for the swing motion to identify the parameters. Physical measurements, computer-aided design (CAD) software, and system identification experiments are used to obtain the parameters of the grey box model. The pendulum-like grey box model is linearized with identified parameters for future controller design. The linearized dynamics model is then validated with experimental data.

The swing oscillation is a shared issue among most indoor miniature blimps. For many indoor blimps such as [25], the center of mass (CM) is located below the center of buoyancy (CB) for better stability [6]. Moreover, the thrusters are usually installed beneath the envelop for weight reduction and better alignment. As a consequence, the undesired pitching or rolling torque, and thus swing oscillation is inevitable once the thrusters are on. Therefore, identification of the rotational dynamics would be widely needed for many other indoor miniature blimps.

This paper is organized as follows: in Section II, we present the GT-MAB platform and the structure of the dynamics model. In Section III, parameters of the dynamics model are identified through measurement, CAD modeling, and system identification experiments. In Section IV, the model is linearized and then validated with experimental data. In Section V, we draw the conclusion and discuss future work.

II. GT-MAB and Dynamics Model

A. Coordinate Systems and Generic Dynamics Model

Following the same convention as our previous work [6], we define the coordinate systems as shown in Fig. 2. The inertial frame is denoted as $O_I - X_I Y_I Z_I$ with axis Z_I pointing downward. The body frame $O_B - X_B Y_B Z_B$ is fixed to GT-MAB while the origin O_B is located at the center of volume (CV) of the envelop. Due to the symmetric "saucer-shaped" envelop of GT-MAB, the CV coincides with the center of buoyancy (CB). Let $\boldsymbol{\eta}^I = [\dot{x}, \dot{y}, \dot{z}]^\top$ and $\boldsymbol{\eta}^B = [u, v, w]^\top$ represent the linear velocity in inertial and body-fixed frame, and ϕ, θ, ψ represent Euler angles for the roll, pitch, and yaw of GT-MAB repectively. Let $\boldsymbol{\omega} = [p, q, r]^\top$ be the angluar velocity of GT-MAB in body-fixed frame. The 6-DOF dynamics for GT-MAB can be presented as:

$$\begin{aligned} m(\dot{\boldsymbol{\eta}}^B + \boldsymbol{\omega} \times \boldsymbol{\eta}^B) &= \boldsymbol{F} + \boldsymbol{f} \\ \boldsymbol{I}\dot{\boldsymbol{\omega}} + \boldsymbol{\omega} \times (\boldsymbol{I}\boldsymbol{\omega}) &= \boldsymbol{M} + \boldsymbol{\tau}, \end{aligned} \tag{1}$$

where m is the total mass of the blimp, including the mass of the helium gas inside the envelop. The terms $\boldsymbol{f} = [f_x, f_y, f_z]^\top$ and $\boldsymbol{\tau} = [\tau_x, \tau_y, \tau_z]^\top$ are translational forces and moments generated by the thrusters. Let $\boldsymbol{F} = [F_x, F_y, F_z]^\top$ and $\boldsymbol{M} = [M_x, M_y, M_z]^\top$ represent the sum of forces and moments due to gravity, buoyancy, and other aerodynamic forces acting on the blimp. The terms $\boldsymbol{f}$, $\boldsymbol{\tau}$, $\boldsymbol{F}$, and $\boldsymbol{M}$ are all defined in the body-fixed frame. The symbol $\boldsymbol{I}$ represents a 3 by 3 matrix for the moment of inertia about center of mass, which is defined as:

$$\boldsymbol{I} = \begin{bmatrix} I_x & -I_{xy} & -I_{xz} \\ -I_{yx} & I_y & -I_{yz} \\ -I_{zx} & -I_{zy} & I_z \end{bmatrix}. \tag{2}$$

B. Physical Design of GT-MAB and Model Simplification

As shown in Fig. 1, GT-MAB consists of a saucer-shaped envelop with a 3D printed gondola underneath. There are five thrusters installed on the gondola to generate linear force along body frame axes and steering torque about Z_B, which are f_x, f_y, f_z and τ_z. Since the thrusters are installed below CV, the undesired torque about X_B and Y_B axes, namely τ_x and τ_y, are inevitable during flight. Positions of

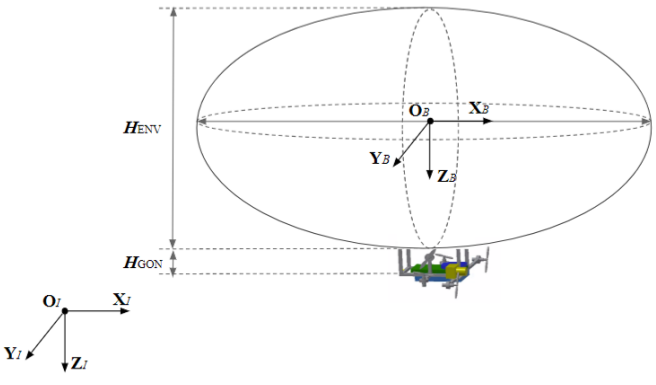

Fig. 2. Inertial and body coordinates setup. Height of the envelop and the gondola are also denoted on the plot as H_{ENV} and H_{GON}.

the components that are mounted on the gondola, such as the battery, are designed to assure that the center of mass (CM) of the gondola is on Z_B. Owing to this symmetrical design, inertia matrix of GT-MAB can be simplified as diagonal with $I_x = I_y$. Similarly, the term $\boldsymbol{\omega} \times (\boldsymbol{I}\boldsymbol{\omega})$ in Equation (1) can be neglected [6]. Therefore, the roll, pitch and yaw motion of the GT-MAB in Equation (1) can be simplified as:

$$\begin{bmatrix} I_x & 0 & 0 \\ 0 & I_y & 0 \\ 0 & 0 & I_z \end{bmatrix} \dot{\boldsymbol{\omega}} = \begin{bmatrix} M_x \\ M_y \\ M_z \end{bmatrix} + \begin{bmatrix} \tau_x \\ \tau_y \\ \tau_z \end{bmatrix}. \tag{3}$$

Thus the pitching and rolling motion can be represented as:

$$\begin{aligned} I_x \dot{p} &= M_x + \tau_x \\ I_y \dot{q} &= M_y + \tau_y \end{aligned}. \tag{4}$$

C. Pendulum-like Dynamics Model for Pitching Motion

Due to the symmetric design of GT-MAB, pitching and rolling dynamics of the robot are almost identical. Therefore we focus on modeling only the pitching oscillation in this paper. For simplicity, we assume the CM of GT-MAB is the pivot of the pitching oscillation, and the translational velocity at CM in inertial frame, $\boldsymbol{\eta}^I_{\mathrm{CM}} = [\dot{x}, \dot{y}, \dot{z}]^\top = [0,0,0]^\top$. Moreover, the Euler angle and angular velocity of GT-MAB, are assumed to be $[\phi, \theta, \psi]^\top = [0, \theta, 0]^\top$ and $\boldsymbol{\omega} = [0, q, 0]^\top$ separately. Thus, Y_B is parallel with Y_I axis, and GT-MAB is pitching with angular velocity $q = \dot{\theta}$.

As shown in Fig. 3, the pitching oscillation of GT-MAB is demonstrated with the side view of the robot. We denote F_{B} as the total buoyancy applied on CV, and F_{G} as the gravitational force at CM separately. Thrust force in X_B direction is represented as $f_x(u)$, where u is the control command to the corresponding motors. The thruster-induced torque about the CM is denoted as τ_{T}. Similarly, the moment of inertia, gravitational restoring torque and air damping moment about the CM are represented as I_{CM}, M_{G}, and M_{d} separately. The distance between CV and CM is denoted as d_{VM}, while that between $f_x(u)$ and CM is denoted as d_{MT}. Similarly, the distance between the between CV and $f_x(u)$ is represented as d_{VT}. Therefore, the pitching oscillation about the CM can be written as:

$$I_{\mathrm{CM}} \dot{q} = I_{\mathrm{CM}} \ddot{\theta} = M_{\mathrm{d}} + M_{\mathrm{G}} + \tau_{\mathrm{T}}. \tag{5}$$

The aerodynamic damping term, M_{d}, can be assumed to be linear to angular velocity $\dot{\theta}$ for the low-speed indoor blimps [26]. Denote b as the damping coefficient, and M_{d} can be found as:

$$M_{\mathrm{d}} = -bq = -b\dot{\theta}. \tag{6}$$

The gravitational restoring torque, M_{G}, stabilizes the blimp given that CM is below CB. This stabilization moment, M_{G}, can be represented as:

$$M_{\mathrm{G}} = -F_{\mathrm{B}} d_{\mathrm{VM}} \sin(\theta). \tag{7}$$

The pitching moment induced by the thrusters, τ_{T}, can be found as:

$$\tau_{\mathrm{T}} = d_{\mathrm{MT}} f_x(u). \tag{8}$$

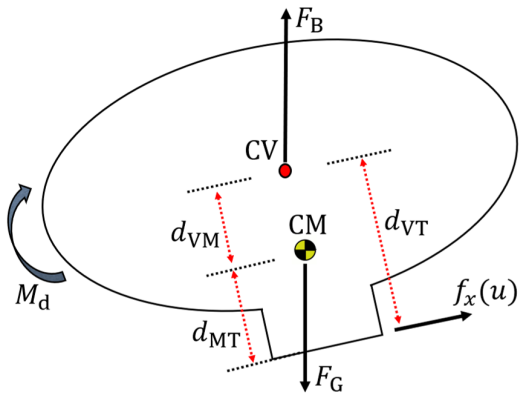

Fig. 3. Side view of GT-MAB. Forces and moments that contribute to the pitching oscillation are annotated on the plot.

Therefore, the dynamics model in Equation 5 can be written as:

$$I_{\mathrm{CM}} \ddot{\theta} = -b\dot{\theta} - F_{\mathrm{B}} d_{\mathrm{VM}} \sin(\theta) + d_{\mathrm{MT}} f_x(u). \tag{9}$$

As illustrated in Fig 3, the term d_{MT} in Equation (9) can be written as $d_{\mathrm{MT}} = d_{\mathrm{VT}} - d_{\mathrm{VM}}$, where d_{VT} is a constant parameter from the dimension measurements in Section III-A. GT-MAB is neutrally ballasted prior to each flight, thus we can assume that the total buoyancy F_{B} is equal to the total gravitational force, $F_{\mathrm{B}} = F_{\mathrm{G}} = mg$, where g is gravitational constant. Therefore, the pitching dynamics described in Equation (9) can be written as:

$$I_{\mathrm{CM}} \ddot{\theta} = b\dot{\theta} - d_{\mathrm{VM}} \sin(\theta) mg - (d_{\mathrm{VT}} - d_{\mathrm{VM}}) f(u). \tag{10}$$

D. Grey Box Model

The terms d_{VM}, d_{VT}, m, and $f(u)$ in Equation (9) can be calculated or measured with relatively good accuracy. However, the air damping coefficient b and the moment of inertia I_{CM} cannot be easily estimated due to the complex aerodynamics effects and the non-ideal geometry of the envelop. Therefore, a grey box model is constructed to identify the parameters b and I_{CM}:

$$\begin{aligned} \dot{x_1} &= x_2 \\ \dot{x_2} &= [-bx_2 - mgd_{\mathrm{VM}} \sin(x_1) + (d_{\mathrm{VT}} - d_{\mathrm{VM}}) f(u)] / I_{\mathrm{CM}}, \end{aligned} \tag{11}$$

where $\boldsymbol{x} = [\theta, \dot{\theta}]^\top$, which are the angle and angular rate of the pitching motion separately. Identification of the parameters in the above model will be presented in Section III.

III. Parameter Identification

A. g and d_{VT}

g is known as gravitational constant, we take $9.81\mathrm{m/s}^2$ for our calculation. d_{VT} is the distance between the center of volume (CV) and the thrust force $f_x(u)$. GT-MAB can be considered as a rigid body when inflated, therefore d_{VT} is a constant parameter and can be calculated as:

$$d_{\mathrm{VT}} = H_{\mathrm{ENV}}/2 + H_{\mathrm{GON}}, \tag{12}$$

where H_{ENV} and H_{GON} are the height of the envelop and the gondola separately, as illustrated in Fig. 2. With the height

measurement $H_{\text{ENV}} = 0.44\text{m}$ and $H_{\text{GON}} = 0.04\text{m}$, we have $d_{\text{VT}} = 0.26\text{m}$.

B. $f_x(u)$

$f_x(u)$ represents the mapping between the motor thrust and the input command. The command $u \in [-1,1]$ represents the duty circle that controls the DC motor of GT-MAB. Positive u will results the motor thrust in X_B direction, while negative value will generate force oppositely. Neglecting the resistance of the electronics such as H-bridge, we can approximate the voltage applied on the motor as:

$$V_{\text{motor}} = V_{\text{batt}} \cdot u, \tag{13}$$

where V_{batt} is the voltage of the battery, which can be measured by the circuitry on GT-MAB. Similar as the work [26], we measure the motor thrust with a high-accuracy scale. The relationship between the motor thrust and the applied voltage can be seen in Fig. 4.

C. m

Total mass of GT-MAB, m, is hard to be directly measured since the helium gas inside the envelop cannot be easily gauged. Instead, by measuring the lifting force provided by the envelop, we can derive the total buoyancy of GT-MAB, and therefore find the total mass of the vehicle. Let F_{lift} be the lifting force provided by the envelop, which is equal to the total buoyancy F_{B} minus the gravitational forces of the helium gas and the deflated envelop. Moreover, since GT-MAB is neutrally buoyant, F_{lift} equals to the gravitational force of all the components that are attached on the envelop, thus the gondola assembly, the ballast weight, and the localization trackers. Therefore, F_{B} and F_{lift} can be represented as follows:

$$\begin{aligned} F_{\text{lift}} &= F_{\text{B}} - (m_{\text{envelop}} + m_{\text{helium}})g \\ &= (m_{\text{gondola}} + m_{\text{tracker}} + m_{\text{ballast}})g \end{aligned} \tag{14}$$

$$\begin{aligned} F_{\text{B}} &= (m_{\text{envelop}} + m_{\text{helium}})g \\ &+ (m_{\text{gondola}} + m_{\text{tracker}} + m_{\text{ballast}})g, \end{aligned} \tag{15}$$

where m_{envelop}, m_{helium}, m_{gondola}, m_{tracker}, m_{ballast} are the mass of the deflated envelop, helium gas, gondola assembly, localization tackers, and the ballast weight separately.

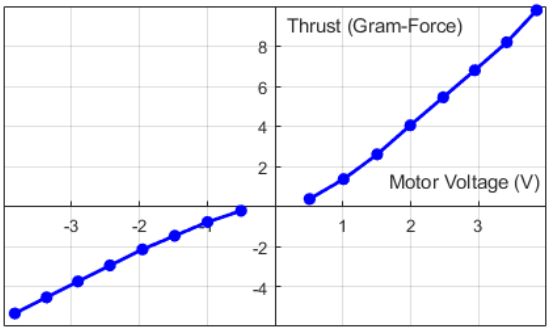

Fig. 4. Motor thrust in X_B direction, versus the voltage applied on the motors, V_{motor}.

According to Archimedes' principle, and assuming the envelop dominates the volume of GT-MAB, we can find that the total buoyancy F_{B} is equal to the weight of air that the envelop displaces. Then, Equation (15) for F_{B} can be written as:

$$\begin{aligned} F_{\text{B}} &= \rho_{\text{air}} V_{\text{envelop}} g \\ &= (m_{\text{envelop}} + m_{\text{helium}})g \\ &+ (m_{\text{gondola}} + m_{\text{tracker}} + m_{\text{ballast}})g, \end{aligned} \tag{16}$$

where ρ_{air} and V_{envelop} are the density of air and the volume of the envelop respectively. Given that the mass of the helium gas is:

$$m_{\text{helium}} = \rho_{\text{helium}} V_{\text{helium}} = \rho_{\text{helium}} V_{\text{envelop}}, \tag{17}$$

the volume of the envelop can be calculated as:

$$V_{\text{envelop}} = \frac{m_{\text{gondola}} + m_{\text{tracker}} + m_{\text{ballast}} + m_{\text{envelop}}}{\rho_{\text{air}} - \rho_{\text{helium}}}. \tag{18}$$

Assuming the temperature of the indoor environment is around 300K (26.85°C), density of both helium and air is known as $\rho_{\text{helium}} = 0.164\text{kg/m}^3$ and $\rho_{\text{air}} = 1.161\text{kg/m}^3$. With the mass measurement from Table I, the total mass of GT-MAB, m, can be calculated as:

$$m = \rho_{\text{air}} V_{\text{envelop}} = 0.1249\text{kg}. \tag{19}$$

D. d_{VM} and initial approximation of I_{CM}

With the mass of all components of GT-MAB measured or calculated in previous sections, we use CAD software to calculate the position of the CM, d_{VM}, and the rough estimate of the moment of inertia, I_{CM}. The estimated I_{CM} will be used as the initial approximation for the system identification experiments in Section III-E.

As illustrated in Fig. 5, the envelop of GT-MAB is modeled as an ellipsoid in the CAD software. From the work [27], dimension of the inflated envelop can be calculated by its deflated radius as:

$$\begin{aligned} r_{\text{inflated}} &\approx 0.7627 r_{\text{deflated}} \\ \tau_{\text{inflated}} &\approx 0.9139 r_{\text{deflated}} \end{aligned} \tag{20}$$

where r_{deflated} is the radius of the deflated envelop, and r_{inflated} and τ_{inflated} are the radius and thickness of the inflated envelop separately. For simplicity, the ellipsoid CAD model is constructed with the same dimension. With the measured radius of the deflated envelop, $r_{\text{deflated}} = 0.457\text{m}$, we found that $d_{\text{VM}} = 0.0971\text{m}$ and $I_{\text{CM}} = 0.00371\text{kg} \cdot \text{m}^2$ through Autodesk Inventor software [28].

TABLE I
MASS MEASUREMENT OF THE COMPONENTS OF GT-MAB

Parameters	Measured Mass
m_{gondola}	52.5 grams
m_{envelop}	38.8 grams
m_{tracker}	7.452 grams
m_{ballast}	8.489 grams

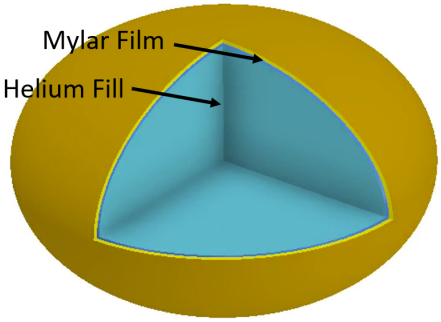

Fig. 5. CAD modeling of the helium-filled envelop.

E. I_{CM} and b

Now I_{CM} and b are the only two unknown parameters in the grey box model described in Equation (11). A series of system identification experiments are designed to obtain these parameters. GT-MAB is released with initial pitch angle θ_0, and the motion capture system (OptiTrack) logs the free response of the pitching oscillation. The experiment is repeated eight times with different initial angle θ_0. The first seven datasets are used for identifying the parameters and the last one is for validation.

As listed in Table II, seven I_{CM} and b pairs are identified from the first seven datasets with MATLAB System Identification Toolbox [29]. Fig. 6 demonstrates both the logged pitch angle and the simulated response with the identified parameters from the first dataset. The fitting between the measured and modeled system is quantified as normalized root-mean-square error (NRMSE). The final estimations of I_{CM} and b are found as the average from the seven identified results in Table II, which are $I_{CM} = 0.005821\text{kg}\cdot\text{m}^2$ and $b = 0.000980\text{N}\cdot\text{m}\cdot\text{s/rad}$.

F. Identified Dynamics Model

Table III summarizes the parameters of the dynamics model obtained from the previous sections. Therefore, the pitching dynamics model of GT-MAB in Equation (10) can be represented as:

$$\ddot{\theta} = -20.4284\sin(\theta) - 0.1684\dot{\theta} + 27.9933 f(u). \tag{21}$$

IV. Linearization and Validation

The identified model is then linearized around $\theta = \dot{\theta} = 0$ for future controller design. State-space form of the linearized model can be written as:

$$\begin{bmatrix}\dot{x_1}\\ \dot{x_2}\end{bmatrix} = \begin{bmatrix}0 & 1\\ -20.4284 & -0.1684\end{bmatrix}\begin{bmatrix}x_1\\ x_2\end{bmatrix} + \begin{bmatrix}0\\ 27.9933\end{bmatrix} f(u), \tag{22}$$

where $\boldsymbol{x} = [\theta, \dot{\theta}]^\top$. This linearized model is compared with the eighth dataset discussed in Section III-E for validation. The linearized model has a satisfying 88.37% NRMSE fit with the validation data, which can be seen in Fig. 7.

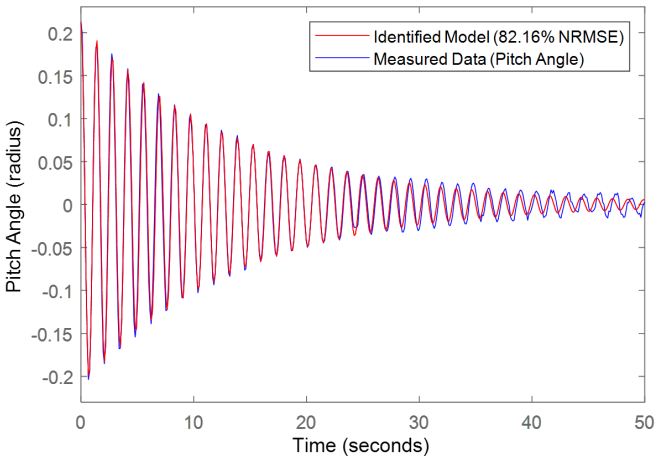

Fig. 6. Measured pitching oscillation and the simulated response with the identify parameters from dataset 1.

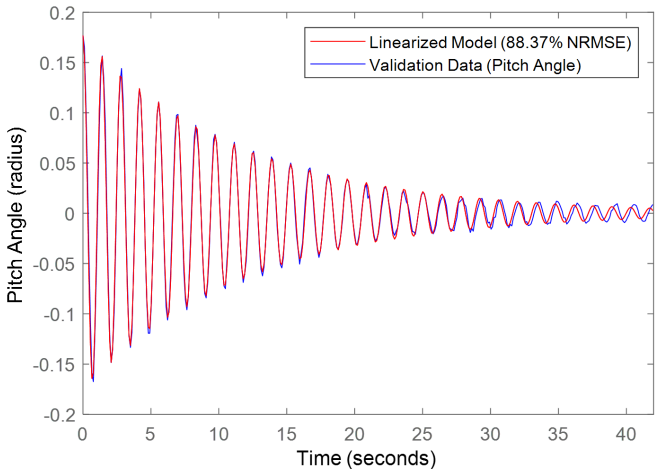

Fig. 7. Measured pitching oscillation from the validation dataset and the simulated response with the linearized dynamics model.

TABLE II
Parameters Identified from the Experimental Datasets

	I_{CM}	b	NRMSE Fit
Dataset 1	0.005782	0.000838	82.16%
Dataset 2	0.005847	0.000978	85.45%
Dataset 3	0.005835	0.000940	84.29%
Dataset 4	0.005828	0.001140	85.20%
Dataset 5	0.005851	0.001083	87.26%
Dataset 6	0.005750	0.001025	77.80%
Dataset 7	0.005855	0.000857	85.21%
Mean	0.005821	0.000980	83.91%

TABLE III

PARAMETERS FOR GT-MAB'S PITCHING DYNAMICS MODEL

Parameters	Value
g	9.81 $\mathrm{m/s^2}$
I_{CM}	0.005821 $\mathrm{kg \cdot m^2}$
b	0.000980 $\mathrm{N \cdot m \cdot s/rad}$
m	0.1249 kg
d_{VT}	0.26 m
d_{VM}	0.097051 m

V. CONCLUSIONS AND FUTURE WORKS

This work identifies the parameters of the rotation-related dynamics of GT-MAB. Linearizion of the dynamics model is also presented for future controller design. The linearized model with identified parameters shows satisfactory fit with the validation data.

We plan to finalize the 6DOF model of GT-MAB by investigating the coupling between the translational and rotation dynamics of the robot. The autopilot of GT-MAB will also be updated to reduce the swing oscillation during flight.

VI. ACKNOWLEDGMENTS

The authors would like to show the heartfelt gratitude to Sean Maxon and Chang Qin for helping with the experiments and building the GT-MAB prototype.

REFERENCES

[1] D. St-Onge, P.-Y. Brches, I. Sharf, N. Reeves, I. Rekleitis, P. Abouzakhm, Y. Girdhar, A. Harmat, G. Dudek, and P. Gigure, "Control, localization and human interaction with an autonomous lighter-than-air performer," *Robotics and Autonomous Systems*, vol. 88, pp. 165 – 186, 2017.

[2] Y. Bestaoui Sebbane, *Lighter than air robots*. Springer Netherlands, 2012.

[3] T. Takaya, H. Kawamura, Y. Minagawa, M. Yamamoto, and A. Ohuchi, "Pid landing orbit motion controller for an indoor blimp robot," *Artificial Life and Robotics*, vol. 10, no. 2, pp. 177–184, Nov 2006.

[4] Q. Tao, M. King-Smith, A. Muni, V. Mishra, S. Cho, P. Varnell, and F. Zhang, "Control theory - autonomous blimp," in *IEEE CSS Video Clip Contest*, 2015.

[5] Q. Tao, V. Mishra, P. Cheng, S. Cho, J. Varnell, and F. Zhang, "Autonomous indoor robotic blimps for research and education," US Provisional Patent 62/632,624, 02 20, 2018.

[6] S. Cho, V. Mishra, Q. Tao, P. Varnell, M. King-Smith, A. Muni, W. Smallwood, and F. Zhang, "Autopilot design for a class of miniature autonomous blimps," in *Proc. of IEEE Conference on Control Technology and Applications (CCTA)*, 2017.

[7] N. Yao, E. Anaya, Q. Tao, S. Cho, H. Zheng, and F. Zhang, "Monocular vision-based human following on miniature robotic blimp," in *IEEE International Conference on Robotics and Automation (ICRA)*, 2017.

[8] A. G. Kendall, N. N. Salvapantula, and K. A. Stol, "On-board object tracking control of a quadcopter with monocular vision," in *2014 International Conference on Unmanned Aircraft Systems (ICUAS)*, May 2014, pp. 404–411.

[9] Y. Li, M. Nahon, and I. Sharf, "Airship dynamics modeling: A literature review," *Progress in Aerospace Sciences*, vol. 47, no. 3, pp. 217 – 239, 2011.

[10] S. B. V. Gomes and J. G. Ramos, "Airship dynamic modeling for autonomous operation," in *Proceedings of IEEE International Conference on Robotics and Automation*, 1998.

[11] T. Lutz, P. Fund, A. Jakobi, and S. Wagner, "Summary of aerodynamic studies on the lotte airship," in *Proceeding of the 4th international airship convention and exhibition*, July 2002.

[12] X. Wang, G. Fu, D. Duan, and X. Shan, "Experimental investigations on aerodynamic characteristics of the zhiyuan-1 airship," *Journal of Aircraft*, vol. 47, no. 4, pp. 1463–1468, 2010.

[13] S. Kale, P. Joshi, and R. Pant, "A generic methodology for determination of drag coefficient of an aerostat envelope using cfd," *AIAA 5th ATIO and 16th Lighter-Than-Air Sys Tech. and Balloon Systems Conferences*, 2005.

[14] P. Gonzlez, W. Burgard, R. Sanz Domnguez, and J. Lpez Fernndez, "Developing a low-cost autonomous indoor blimp," *Journal of Physical Agents (JoPha)*, vol. 3, no. 1, pp. 43–52, 2009.

[15] S. B. i Badia, P. Pyk, and P. F. M. J. Verschure, "A biologically based flight control system for a blimp-based UAV," in *Proceedings of the 2005 IEEE International Conference on Robotics and Automation*, April 2005, pp. 3053–3059.

[16] T. Takaya, H. Kawamura, Y. Minagawa, M. Yamamoto, and A. Ouchi, "Motion control in three dimensional round system of blimp robot," in *2006 SICE-ICASE International Joint Conference*, Oct 2006, pp. 1291–1294.

[17] H. Kawamura, M. Yamamoto, T. Takaya, and A. Ohuchi, "Learning landing control of an indoor blimp robot for self-energy recharging," *Artificial Life and Robotics*, vol. 12, no. 1, pp. 116–121, Mar 2008.

[18] H. Kawamura, H. Iizuka, T. Takaya, and A. Ohuchi, "Cooperative control of multiple neural networks for an indoor blimp robot," *Artificial Life and Robotics*, vol. 13, no. 2, pp. 504–507, Mar 2009.

[19] M. Mahn and M. Kemper, "A behaviour-based navigation system for an autonomous indoor blimp," *IFAC Proceedings Volumes*, vol. 39, no. 16, pp. 837 – 842, 2006, 4th IFAC Symposium on Mechatronic Systems.

[20] F. Hayato and S. Akira, "Wind-disturbance-based control approach for blimp robots," *Electronics and Communications in Japan*, vol. 97, no. 2, pp. 52–59.

[21] C. Wan, N. Kingry, and R. Dai, "Design and autonomous control of a solar-power blimp," in *2018 AIAA Guidance, Navigation, and Control Conference, AIAA SciTech Forum*, 2018.

[22] Y. Wang, G. Zheng, D. Efimov, and W. Perruquetti, "Altitude control for an indoor blimp robot," *IFAC-PapersOnLine*, vol. 50, no. 1, pp. 15 990 – 15 995, 2017, 20th IFAC World Congress.

[23] J.-C. Zufferey, A. Guanella, A. Beyeler, and D. Floreano, "Flying over the reality gap: From simulated to real indoor airships," *Autonomous Robots*, vol. 21, no. 3, pp. 243–254, Nov 2006.

[24] D. Palossi, "Self-sustainability in nano unmanned aerial vehicles: A blimp case study," in *CF'17 Proceedings of the Computing Frontiers Conference*, 2017.

[25] V. Srisamosorn1, N. Kuwahara, A. Yamashita1, T. Ogata, and J. Ota, "Design of face tracking system using fixed 360-degree cameras and flying blimp for health care evaluation," in *The 4th International Conference on Serviceology*, 2016.

[26] J. Shan, "Dynamic modeling and vision-based control for indoor airship," in *International Conference on Mechatronics and Automation*, 2009.

[27] I. M. Mladenov, "On the geometry of the mylar balloon," *Comptes Rendus de l'Academie Bulgare des*, 2001.

[28] "About mass properties," Autodesk Knowledge Network, [Accessed: 28- Jun- 2018].

[29] L. Ljung, *System Identification Toolbox User's Guide*, MathWorks, Inc, 3 Apple Hill Drive Natick, MA 01760-2098, 3 2018.